Submitted to Physical Review D

E-395

FERMILAB-PUB-78-183-E
UPR-39E (Revised)
University of Pennsylvania
August, 1978

π^+ STRUCTURE INFORMATION FROM A JET EXPERIMENT

M. Dris,[3] M. D. Corcoran,[4] L. Cormell,[3] A. R. Erwin,[4]
P. J. Gollon,[1] E. H. Harvey,[4] A. Kanofsky,[2] W. Kononenko,[3]
B. Robinson,[3] W. Selove,[3] M. Thompson,[4] and B. Yost[3]

[1]Fermilab, Batavia, Illinois 60510
[2]Lehigh University, Bethlehem, Pa. 18015
[3]University of Pennsylvania, Philadelphia, Pa. 19104, and
[4]University of Wisconsin, Madison, Wisconsin 53706

ABSTRACT

In a double-arm jet experiment, we have studied two-jet events in π^+p and pp collisions. We analyze the data using a parton scattering model and obtain a quark-anti-quark structure function for the pion.

INTRODUCTION

Bjorken[1] has discussed the possibility of measuring the hadron structure functions and $d\sigma/dt'$, the parton-parton scattering cross section, from hadron-hadron collisions. We have recently performed a jet experiment studying πp and pp collisions leading to high-p_T final states.[2,3,4] In this paper we examine the ratio of the di-jet cross sections:

$$\frac{\sigma_p}{\sigma_\pi} = \frac{\sigma(pp \to \text{jet L} + \text{jet R} + X)}{\sigma(\pi p \to \text{jet L} + \text{jet R} + X)} \tag{1}$$

over a range of angles and of p_T values. (Here L and R indicate the "left" arm and "right" arm jets respectively.) We assume that all particles detected come from hard scattering of the constituents of the interacting hadrons. The use of double-arm cross sections constrains the kinematical variables involved and simplifies many calculations. We find that the ratio σ_p/σ_π is approximately independent of the x of the colliding "target" parton and of other kinematical variables and depends only on the x of the "beam" parton, where x is the longitudinal momentum of the parton divided by the momentum of the hadron. From this result and some additional assumptions we are able to determine a structure function $f_{(q+\bar{q}),\pi}(x)$ for the pion.

Detector and Beam

The detector was a two-arm calorimeter which is described in further detail in references 2-4. Each arm was segmented in three dimensions. The entire array could be moved longitudinally to change the target to calorimeter distance. Each arm could also be moved transversely to the beam. The data discussed here were taken with positively charged particles at 130 GeV and 200 GeV in the M2 beam at Fermilab. Pions and protons were tagged with Čerenkov counters. The left and right arms were positioned to cover various center of mass angles, as summarized in Table I.

Trigger

The events used for calculating the pion structure function were taken with an "L + R" trigger,[4] with events being recorded when the sum, $p_T(L)+p_T(R)$, was above an adjustable threshold. These events show an unconstrained tendency to give approximate balancing of $\vec{p}_T(L)$ and $\vec{p}_T(R)$; the difference of their magnitudes has a typical standard deviation of approximately 1 GeV/c.[4] The p_T values used in the present analysis ranged from 2.4 to 3.4 GeV/c in each arm.

Data

Data were taken under the three conditions summarized in Table I. Pion and proton-induced events were recorded simultaneously for

each of these conditions, thus eliminating a number of systematic errors. The beam p/π^+ ratio was 1.4 at 130 GeV and 2.4 at 200 GeV.

Jet Containment, Fiducial Region, Coplanarity

The jet model[1,5,6] predicts that some fragments of the jet will be found at large angles from the jet axis. We address here the resulting questions of jet containment and of the achievable accuracy in determining the momentum vector of the jet using a detector of limited solid angle.

To study jet containment we first consider a set of events $p\ (\pi) + p \rightarrow$ Jet R + X taken with a single-arm "R" trigger. For each event we calculate the center of mass angles θ and ϕ of the jets, treating each fragment as massless. We then select a set of jets having $2.4 \leq p_T \leq 2.8$ GeV/c and $75^o \leq \theta_R \leq 93^o$. These cuts select events with the right jet near the center of our region of θ_R coverage. We then plot the ϕ_R distribution of these events, $dN/d\phi_R$, for proton-induced jets ("proton jets") and for pion-induced jets ("pion jets").

The results show that $dN/d\phi_R$ falls, for a given measured $p_T(R)$, as the jet axis goes away from the center of the calorimeter arm (Fig. 1a and b). (We believe that this is caused by a reduced acceptance of our calorimeter for events whose jet axes lie near its edge.) More importantly, we note that $dN/d\phi_R$ falls in almost the same way for proton jets and for pion jets, as shown in Fig. 1c. This observation has several important implications and consequences:

(1) First, it implies that the pion jets and proton jets in this p_T and θ_R range have very similar fragmenting distributions, i.e., very similar multiplicities and similar "sizes".

(2) This observation also implies that the pion jets and proton jets, in this p_T and θ_R range, come from virtually identical constituents. That is, if both quark jets and gluon jets are being detected, and if these jets have different "sizes", then the ratio of quark jets to gluon jets must be quite similar for the observed proton and pion jets.

(3) Because $dN/d\phi_R$ for proton and pion jets have such similar ϕ-dependences, the ratio of cross sections for single-arm jet production,

$$R_1 = \frac{dN(pp \to \text{jet } R + X)/d\phi_R}{dN(\pi p \to \text{jet } R + X)/d\phi_R} \cdot \frac{n_\pi}{n_p}$$

is quite constant over a wide range of ϕ_R, as seen in Fig. 1c. (Here n_π and n_p are the pion and proton beam fluxes.) Since R_1 is a sensitive function of p_T,[4] the fact that it is constant while both $dN/d\phi_R$ drop several-fold suggests that the "true" p_T of the measured jet is not appreciably different from its measured value at larger values of $|\phi_R|$ even though the calorimeter acceptance has dropped by a large factor at these angles. This indicates that the measured p_T of the jet is close to its "true" value until the jet axis comes to within about 20° of the edge of the calorimeter. We interpret that this behavior results from the steepness of the p_T spectrum, which causes the dominant contribution to jets of a given

apparent p_T to come from those jets, of only slightly higher average p_T, which happen to fragment "compactly", i.e., with no fragments more than 30° or so from the jet axis.[7,8]

We have made a similar study of containment using the two-arm "L+R"-triggered events. The results, shown in Fig. 2, are very similar to those for single-arm triggers shown in Fig. 1, and again indicate that the ratio of proton to pion jet cross sections is almost constant over a broad range of ϕ_R even though both cross sections change several-fold over this range. Thus we have evidence that for the double-arm events, just as for the single-arm-trigger ones, proton-induced jets and pion-induced jets have very similar characteristics.

Figures 3a and 3b show $\langle\phi_R\rangle$ versus ϕ_L for double-arm proton and pion jet events when ϕ_L is limited to a small interval. We see effects of coplanarity: $\langle\phi_R\rangle$ changes in correlation with the selected ϕ_L interval. This correlation study shows that, for two typical jets of 2.5 GeV/c each, with $\theta_L = \theta_R = 80^o$, a change of 12° in ϕ_L produces a change of about 4° in the expected direction of ϕ_R. The correlation is less than perfect because of calorimeter acceptance effects and is further reduced by the internal transverse momentum k_T of the partons.

The results shown in figures 1 and 2 and the discussion above indicate that:

(1) For θ_L and θ_R in the central region of their respective calorimeters, the measured momentum and direction of each jet are not seriously different from their true values, and

(2) We can use most of the ϕ range of both arms in studying the σ_p/σ_π ratio. We thus conclude that we can use a region about $40^\circ \times 40^\circ$ in the $80^\circ \times 80^\circ$ right arm and a comparable region in the slightly smaller left arm to get a useful measure of the jet momentum and direction. This conclusion is supported by the observation that when we move the calorimeters physically, the σ_p/σ_π ratio does not change, for a given pair of θ_L and θ_R values, unless, for one of the geometries, the jet is closer than 20° or so to the left or right edge of the calorimeter. Thus the same calorimeter edge effects are observed in θ as in ϕ.

Formalism for Double-Arm Cross Sections

Guided by the analyses of Bjorken[1] and of Ellis and Kislinger,[9] we write the cross section for producing two high-p_T jets via the reaction

Hadron A + Hadron B $\rightarrow$ Jet L + Jet R + X, as

$$\frac{d^2\sigma_{AB}}{dp_T^{\,2}\; d(\cos\theta_L)\; d(\cos\theta_R)} =$$

$$\sum_{ij}\left[f_{iA}(x_1)\; f_{jB}(x_2)\frac{d\sigma_{ij}}{dt'}(s',t')\right]\frac{C_{AB}}{\sin^2\theta_L\,\sin^2\theta_R} \qquad (2)$$

This form assumes that coplanar events are selected and that $p_T(L) = p_T(R)$. Here s' and t' are the Mandelstam variables for the parton-parton interaction, and the sum is over all partons in each

hadron. The treatments in references 1 and 9 do not take into account the effects of the initial transverse momentum, k_T, of the colliding partons. We introduce the factor C_{AB} in Eq. 2 to take account of both the inequality of $\vec{p}_T(L)$ and $-\vec{p}_T(R)$, resulting from the initial transverse momentum of the colliding partons, and the effects of detector acceptance, including the $\Delta\phi$ bites. We have ignored scale-breaking effects, which, in general, introduce Q^2 (momentum-transfer squared) dependences. Our convention is that the structure functions f(x) satisfy the normalization conditions

$$\sum_i f_i(x)dx = 1$$

In a simplified view of the parton + parton → jet + jet process, we could neglect "binding energy" effects which presumably cause the jet energy to be less than the energy of the scattered parton, neglect non-zero mass effects for jets, and take the k_T (initial parton transverse momentum) equal to zero. In this approximation the jet momenta $\vec{p}(L)$ and $\vec{p}(R)$ would have equal magnitudes of transverse momentum p_T and would also be coplanar. The parton longitudinal fractional momenta x_1 and x_2 in the hadron-hadron center of mass system would be given by

$$x_1 = \frac{x_T}{2}\left(\cot\frac{\theta_L}{2} + \cot\frac{\theta_R}{2}\right)$$

$$x_2 = \frac{x_T}{2}\left(\tan\frac{\theta_L}{2} + \tan\frac{\theta_R}{2}\right) \qquad (3)$$

where

$$x_T = \frac{2p_T}{\sqrt{s}} \tag{4}$$

We do not know how to exactly correct for the parton "binding energy". We shall therefore ignore its effect. The effect of the non-zero jet masses will be discussed at the end of the paper. We will discuss here some effects of the non-zero k_T.

We note that the two-arm L+R trigger essentially removes the "trigger bias" first discussed by Combridge[10] and gives events with $\vec{p}_T(L) + \vec{p}_T(R)$ centered at zero. However, this trigger does not select events in which the parton transverse momenta are zero.[11] (Even if one selects those few events with $\vec{p}_T(L) + \vec{p}_T(R)$ exactly equal to zero, so that those events have $\vec{k}_T(1) + \vec{k}_T(2)$ equal to zero, they will not in general have $\vec{k}_T(1)$ and $\vec{k}_T(2)$ individually equal to zero.) Because the sum of the observed transverse momenta, $\vec{p}_T(L) + \vec{p}_T(R)$, is non-zero, we have used the modified definition

$$x_T = \frac{p_T(L) + p_T(R)}{\sqrt{s}} \tag{4a}$$

in the present analysis instead of Eq. 4.

The difference in magnitudes of $\vec{p}_T(L)$ and $\vec{p}_T(R)$ gives an approximate measure of the magnitude of k_T, the transverse momentum of each parton. We have noted above that this difference has an RMS value of approximately 1 GeV/c; this implies an RMS value for k_T of approximately 1 GeV/c.[2]

Another effect of non-zero k_T is that the parton-parton momentum transfer t' cannot be uniquely determined from $\vec{p}(L)$ and $\vec{p}(R)$, but instead involves an integral over the "hidden" variables $\vec{k}_T(1)$ and $\vec{k}_T(2)$. This effect is important for the present analysis since the cross section $d\sigma/dt'$ in Eq. 2 must be understood to be an appropriate average over some range of values of $\vec{k}_T$'s. This point must be kept in mind in comparing proton-induced and pion-induced events. In principle the pion and proton $\vec{k}_T$ distributions could be different; and thus the relevant $d\sigma/dt'$ averages could also be different, even for fixed $\vec{p}(L)$ and $\vec{p}(R)$. We studied the imbalance of $\vec{p}_T(L)$ versus $\vec{p}_T(R)$, which reflects the k_T of the partons and found no essential difference between pion and proton jets.

A third effect of non-zero k_T is that the sum of the magnitudes of $\vec{p}(L)$ and $\vec{p}(R)$ will no longer be given just by the sum $(x_1 + x_2)\sqrt{s}/2$. If x_1 and x_2 are still used to represent the longitudinal fractional momenta of the initial partons, then $p(L) + p(R)$ will in general be larger than $(x_1 + x_2)\sqrt{s}/2$, assuming massless jets. However, for the typical events analyzed here, with $p_T \simeq 3$ GeV/c, we estimate that changing $\vec{k}_T$ from 0 to 1 GeV/c would typically change x_1 by only 3 percent.[12]

We return to Eq. 2. In general, the ratio of two-jet cross sections defined in Eq. 1 has the form

$$\frac{\sigma_p}{\sigma_\pi} = \frac{\sum_{ij} f_{ip}(x_1) f_{jp}(x_2) \left\langle \frac{d\sigma_{ij}}{dt'}(s',t') \right\rangle}{\sum_{ij} f_{i\pi}(x_1) f_{jp}(x_2) \left\langle \frac{d\sigma_{ij}}{dt'}(s',t') \right\rangle} \qquad (5)$$

where the averages are carried out over k_T as discussed above. We have chosen to neglect any difference between C_{pp} and $C_{\pi p}$. This cross section ratio is in general a function of x_1, x_2, s' and t'. If only one species of parton were present in the incident particle, Eq. 5 would reduce to

$$\frac{\sigma_p}{\sigma_\pi} = \frac{f_p(x_1)}{f_\pi(x_1)} \tag{6}$$

and this ratio would be a function of only x_1. In the next section, we show that for our data σ_p/σ_π is approximately independent of the target x (i.e. x_2) and of other kinematical variables and depends almost entirely on x_1. We therefore proceed to use Eq. 6 to make an approximate determination of the structure function of the pion.

Results

We used relations (3) and (4a) to calculate the relevant kinematical variables for each event. The data were binned to give reasonable statistics for each point. We used bins of approximately 0.025 in x_1 and 0.03 to 0.04 in x_T. The results for σ_p/σ_π are given in Table II and are plotted in Fig. 4 (130 GeV/c) and Fig. 5 (200 GeV). We observe from figures 4 and 5 that for each of the two beam energies separately the ratio σ_p/σ_π is approximately independent of x_2 and x_T and that one can fit a smooth curve through all the points. However the "best curves" for the two different energies are not identical, since the 200 GeV points lie approximately 25% below the 130 GeV points.[13]

We will make the approximation

$$\frac{f_{eff,p}(x)}{f_{eff,\pi}(x)} = \frac{\sigma_p}{\sigma_\pi} \tag{7}$$

where f_{eff} denotes an "effective structure function" of each hadron, which includes an average over all partons contributing to the high-p_T reactions studied here. The single-species approximation implied by Eq. 7 is supported both by the fact that σ_p/σ_π is experimentally almost entirely dependent on x_1 and by the jet containment results discussed above. A naive interpretation of the significance of this single-species approximation is that the ratio σ_p/σ_π is approximately the ratio of the quark-like, $(q + \bar{q})$, components of the proton and pion structure functions. This interpretation of our data would be a reasonable one (a) if x_1 was always sufficiently large so that gluons in the "beam" particle play a smaller role than do quarks, or (b) if the particular size of our calorimeter arrays (approximately 1.5 srad each[4]) suppresses the detection of gluon jets, which are expected to be more diffuse than quark jets,[14,15] or (c) if the relation between gluon and quark components discussed in footnote 16 is approximately satisfied.

We thus proceed to calculate a structure function for the $q + \bar{q}$ content of the pion in terms of that for the proton:

$$f_{(q+\bar{q}),\pi}(x) = \frac{f_{(q+\bar{q}),p}(x)}{\sigma_p/\sigma_\pi} \tag{8}$$

Even though the 200 GeV and 130 GeV data have some differences, these differences are not large. We have therefore combined them, using Eq. 8 and taking $f_{(q+\bar{q}),p}(x)$ from Ref. 6. We obtain the values of $f_{(q+\bar{q}),\pi}(x)$ given in Table III. These results are plotted in Fig. 6, along with curves of the $(q+\bar{q})$ pion structure functions obtained from Farrar[17] and from Field and Feynman[6]. Our results indicate that (1) the average x of the quark-like constituents of the pion is higher than that of the proton and (2) the high-x dependence of the pion is relatively flat.

We have also analyzed some of the data with a cut imposed limiting $|p_T(L)-p_T(R)|$ to 0.8 GeV/c and compared the results with those obtained without such a cut. We find no distinguishable difference.

In Fig. 7 we display the results obtained by Dao et al.[18] for the valence quark structure function of the pion, based on data from a dimuon experiment. This figure displays only valence quark or antiquark distributions, while our result in Fig. 6 includes valence and sea distributions for the sum of quarks and antiquarks. The points of Ref. 18 lie above ours, but their x-dependence is similar in shape to ours.

Comment on Non-Zero Jet Mass Effects

In a model in which a parton has a definite mass,[19] it is not possible for both momentum and energy to be conserved in the process of a parton being dressed into a jet. In the preceeding discussion we assumed that momentum is conserved in this process.

The formulae of references 1 and 9, and our Eq. 3, hold only when $E_{jet} = p_{jet}$. For large enough p_{jet} and E_{jet}, one may take $E_{jet} \approx p_{jet}$. At p_T values as low as 2.5 GeV/c, we find that E_{jet} is approximatley 10% higher than p_{jet} in the hadron-hadron c.m. system. If one ignores the k_T-effects and the "binding energy" effects mentioned above, by conserving both energy and momentum for the reaction parton + parton → jet + jet[19] one can (in the case $x_1 = x_2$) define a new variable $y_T \equiv x_T \cdot E_{jet}/p_{jet}$ and use it in place of x_T to calculate x_1 and x_2 in Eq 3. Since for our data y_T is approximately 10% larger than x_T in the hadron-hadron c.m., if we use y_T instead of x_T the entire set of points for the structure function is shifted to higher values by approximately 10%.

ACKNOWLEDGEMENTS

We thank D. Duke and H. Miettinen for a very useful discussion.

This work was supported in part by the U.S. Department of Energy.

FIGURE CAPTIONS

Figure 1: $dN/d\phi_R$ distribution for (a) $pp \rightarrow$ jet + X and (b) $\pi p \rightarrow$ jet + X, at 130 GeV. $p_T(R)$ = 2.4 to 2.8 GeV/c and θ_R = 75° to 93°. The edges of the calorimeter for this θ_R interval are at $\phi_R \approx \pm 43^o$. (c) R_1, the ratio of p to π single-arm jet cross sections, as a function of ϕ_R.

Figure 2: $dN/d\phi_R$ distributions for (a) proton-induced, and (b) pion-induced "L + R" events, with $p_T(L) + p_T(R)$ =4.7 to 5.5 GeV/c, and $\theta_L = \theta_R = 75^o$ to 93°; (c) R_2, the ratio of p to π double-arm jet cross sections as a function of ϕ_R. The data are summed over all values of ϕ_L. The ϕ_R and p_T limits are identical to those of Fig. 1.

Figure 3: Coplanarity effects: $< \phi_R >$ versus ϕ_L for the L + R trigger for (a) protons and (b) pions.

Figure 4: σ_p/σ_π the ratio of cross sections given in Eq. 1, as a function of x_1, the fractional longitudinal momentum of the parton in the incident hadron. These data are for 130 GeV beam energy. Errors shown are statistical errors only.

Figure 5: The same variables as in Fig. 4, but for beam energy of 200 GeV.

Figure 6: The total quark-antiquark structure function for the pion as measured in this experiment. The errors are statistical errors only. The curves are theoretical estimates from references 6 and 17.

Figure 7: Valence quark (or antiquark) distribution from Ref. 18, with fit and uncertainty band in the fit. Theoretical estimates are displayed from references 6 and 17.

TABLE CAPTIONS

Table I: Running conditions for data presented here: beam energy, calorimeter fiducial regions for jet axes in the center of mass of the colliding hadrons, and number of accepted events.

Table II: Ratio of measured jet cross sections. x_T is defined by Eq. 4a; x_1 and x_2 are the beam and target parton longitudinal fractional momentum. σ_p/σ_π is the ratio of di-jet cross sections for p and π beams on hydrogen.

Table III: Quark-antiquark structure function for the pion. In this table values from Table II corresponding to the same x_1 are combined. σ_p/σ_π is the ratio of the di-jet cross sections for protons and pions at each x. $f_{(q+\bar{q}),p}$ is the quark plus antiquark structure function for protons obtained from Reg. 6. $f_{(q+\bar{q}),\pi}$ is the pion structure function for quarks plus antiquarks calculated in this work.

REFERENCES

[1]J. D. Bjorken, Phys. Rev. D8, 4098 (1973).

[2]Evidence for jets, and correlated jets in high p_T events. L. Cormell et al., Fermilab Report 77-89, October 1977 (unpublished).

[3]A preliminary look at hadron structure with a double-arm calorimeter. A. R. Erwin, invited talk presented at Vanderbilt Conference, March 1978 (to be published).

[4]Comparison of high p_T events produced by pions and protons. M. D. Corcoran et al., Phys. Rev. Lett. 41, 9 (1978).

[5]S. Berman, J. Bjorken, and J. Kogut, Phys. Rev. D4, 3388 (1971).

[6]R. D. Field and R. P. Feynman, Phys. Rev. D15, 2590 (1977).

[7]M. Dris, using common jet models, has estimated that for a cone of 30° half-angle, and with the observed steepness of the spectrum from jet production, the apparent jet energy is on the average within 0.2-0.3 GeV of the "true" energy. (To be published in Nucl. Instr. and Methods).

[8]M. D. Corcoran, using a Monte Carlo calculation with a similar jet model, has found results supporting the estimates of Ref. 7.

[9]S. D. Ellis and M. B. Kislinger, Phys. Rev. D9, 2027 (1974).

[10]B. L. Combridge, Phys. Rev. D12, 2893 (1975).

[11]B. Peterson, private communication.

[12]This estimate is made by assuming that the energy of the initial parton is $((x_1\sqrt{s}/2)^2 + k_T^2)^{1/2}$ and that the partons have definite

zero mass and that jets are massless. The resulting shift, typically 0.01 in x_1, is smaller than the kinematical uncertainties associated with the non-zero mass jets, as discussed below in the text.

[13]This difference might correspond to some scale-breaking effect or to effects of the approximations we have made.

[14]D. Duke and H. Miettinen, private communication.

[15]K. Shizuya and S.-H. H. Tye, Fermilab Report, 78-54-THY, June 1978.

[16]M. Dris has noted that in the two-parton-types model suggested by Bjorken (Ref. 1), the factorization implied in going from Eq. 5 to Eq. 6 would be exact if the ratio $f_{gluon}(x)/f_{quark}(x)$ were the same for protons and pion for the x_1 values studied in our data. In that case, Eq. 6 would give the ratio $f_{quark,p}(x)/f_{quark,\pi}(x)$ which would be equal to $f_{gluon,p}(x)/f_{gluon,\pi}(x)$.

[17]Glenys R. Farrar, Nucl. Phys. B77, 429 (1974).

[18]F. T. Dao et al., Phys. Rev. Lett. 39, 1388 (1977), and K. Lai, private communication.

[19]R. D. Field and R. P. Feynman, Nucl. Phys. B136, 1 (1978).

TABLE I

Geometry	Energy GeV	Center of Mass Angle Range θ_L	θ_R	$\Delta\phi$ cut	Number of Events
1	130	60°-90°	54°-90°	40°	6K
2	130	72°-102°	66°-102°	40°	9K
3	200	72°-102°	72°-102°	40°	5K

TABLE II

E_{beam} GeV	x_T	x_1	x_2	σ_p/σ_π
130	.345	.56	.21	.80 ± .13
		.51	.24	.86 ± .09
		.46	.27	1.25 ± .12
		.41	.29	1.30 ± .19
		.37	.32	1.02 ± .29
	.335	.44	.26	1.07 ± .13
		.40	.29	1.40 ± .12
		.36	.32	1.74 ± .15
		.32	.36	2.12 ± .40
	.31	.54	.18	.81 ± .17
		.51	.19	1.10 ± .12
		.46	.22	1.13 ± .08
		.41	.24	1.21 ± .08
		.37	.27	1.32 ± .12
		.34	.29	1.30 ± .25
		.33	.30	1.50 ± .09
		.30	.33	1.65 ± .14
		.27	.36	1.70 ± .29
200	.335	.41	.27	.80 ± .19
		.37	.30	.87 ± .15
		.35	.33	1.52 ± .36
	.31	.38	.25	1.11 ± .18
		.35	.28	1.37 ± .16
		.32	.31	1.20 ± .23
		.29	.34	1.35 ± .33
	.29	.36	.24	1.07 ± .14
		.32	.26	1.18 ± .11
		.29	.29	1.49 ± .17
		.27	.31	1.59 ± .32
	.245	.30	.20	1.12 ± .23
		.27	.22	1.36 ± .22
		.25	.24	1.61 ± .31

TABLE III

x	σ_p/σ_π	$f_{(q+\bar{q}),p}$	$f_{(q+\bar{q}),\pi}$
0.25	1.61 ± 0.31	0.96	0.60 ± 0.12
0.27	1.63 ± 0.20	0.905	0.56 ± 0.07
0.295	1.52 ± 0.10	0.85	0.56 ± 0.04
0.323	1.44 ± 0.07	0.775	0.54 ± 0.03
0.355	1.48 ± 0.08	0.69	0.47 ± 0.025
0.372	1.19 ± 0.08	0.643	0.54 ± 0.04
0.407	1.26 ± 0.06	0.558	0.44 ± 0.02
0.456	1.15 ± 0.06	0.438	0.38 ± 0.02
0.51	0.98 ± 0.07	0.32	0.33 ± 0.02
0.54	0.81 ± 0.17	0.268	0.33 ± 0.07
0.56	0.80 ± 0.13	0.233	0.29 ± 0.05

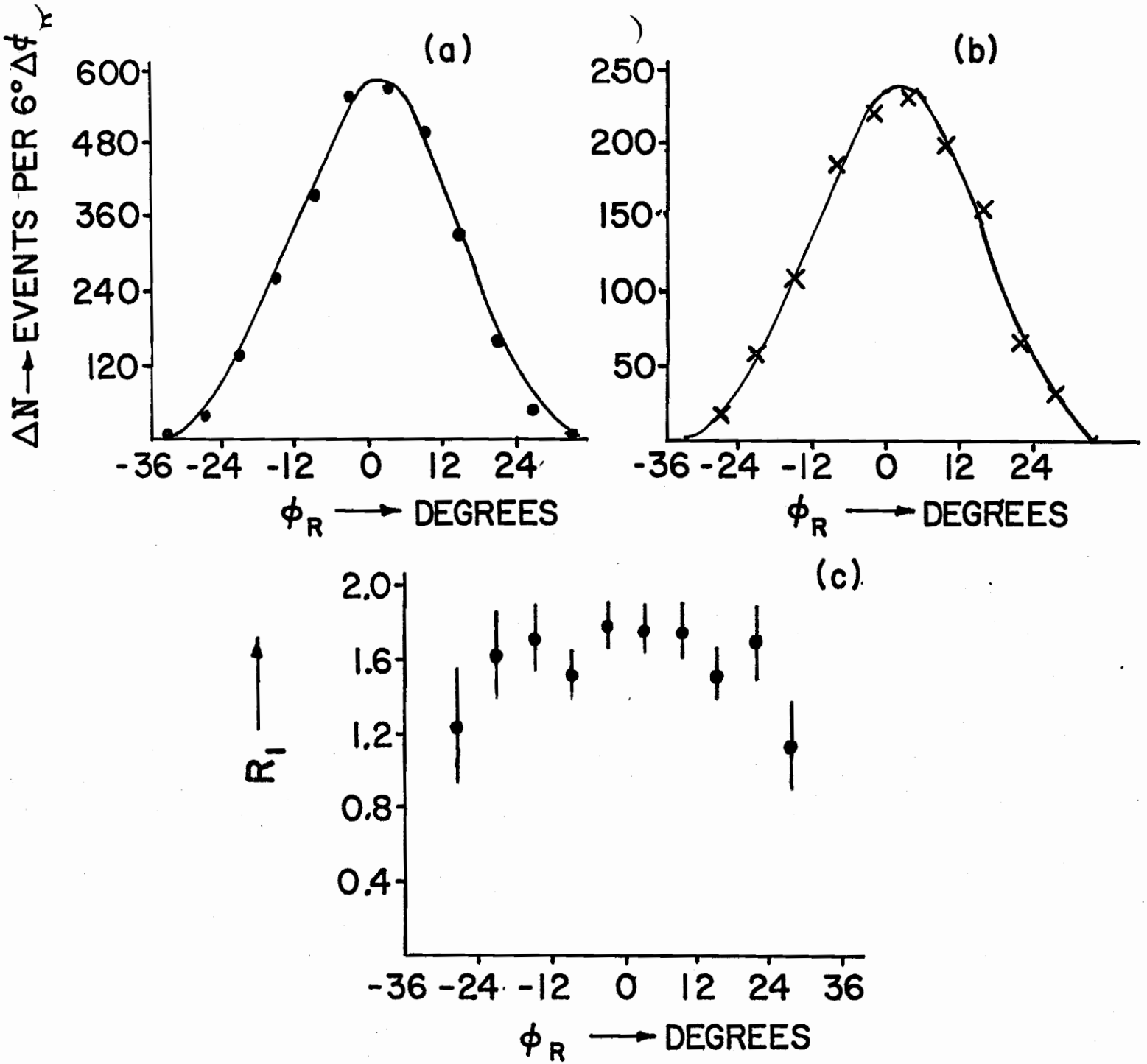
(a)
(b)
(c)
ΔN → EVENTS PER 6° Δφ
600
480
360
240
120
250
200
150
100
50
2.0
1.6
1.2
0.8
0.4
R1
-36 -24 -12 0 12 24
-36 -24 -12 0 12 24 36
φR → DEGREES

FIGURE 1

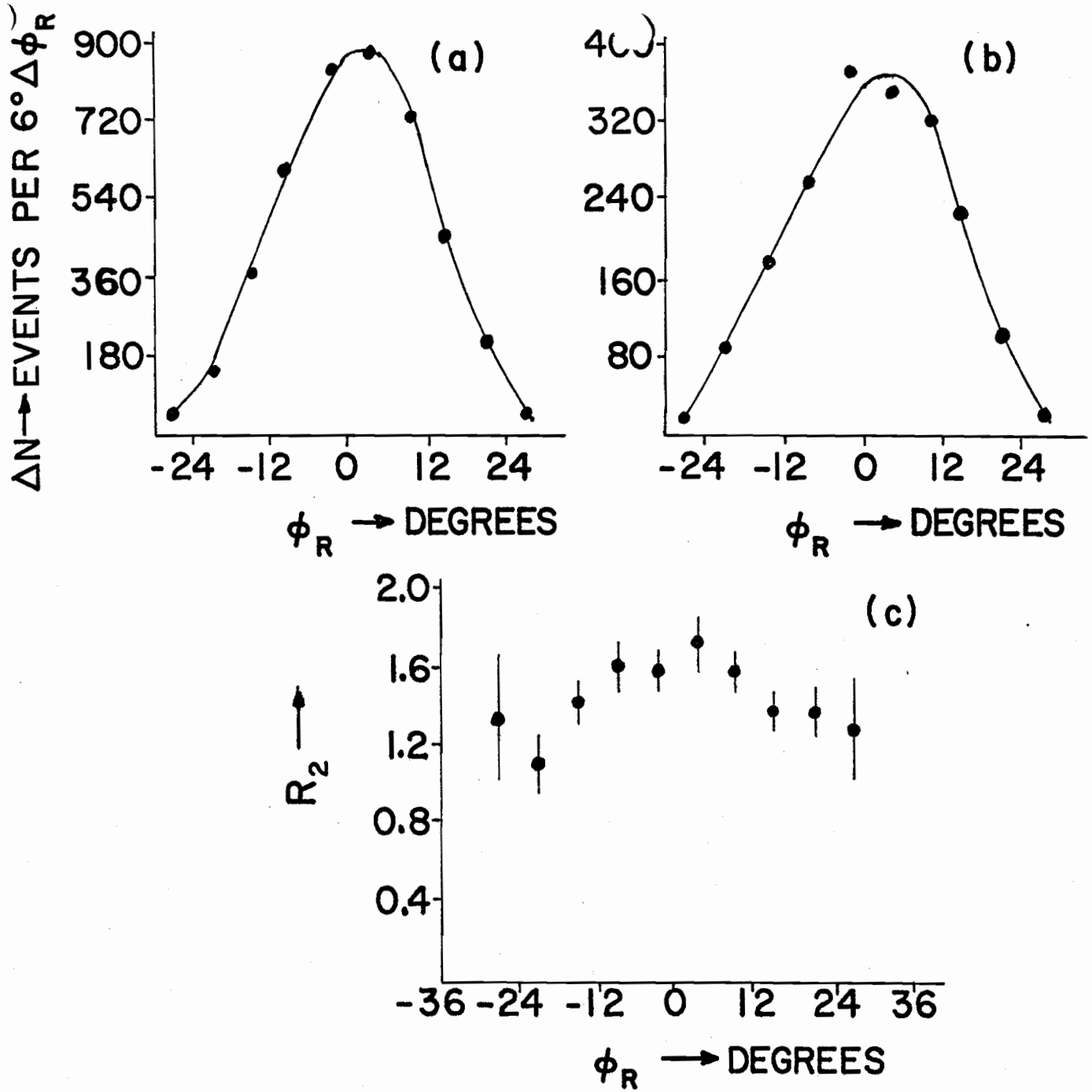
ΔN → EVENTS PER 6° Δφ_R
900
720
540
360
180
(a)
-24 -12 0 12 24
φ_R → DEGREES
320
240
160
80
(b)
-24 -12 0 12 24
φ_R → DEGREES
2.0
1.6
1.2
0.8
0.4
R_2
(c)
-36 -24 -12 0 12 24 36
φ_R → DEGREES

FIGURE 2

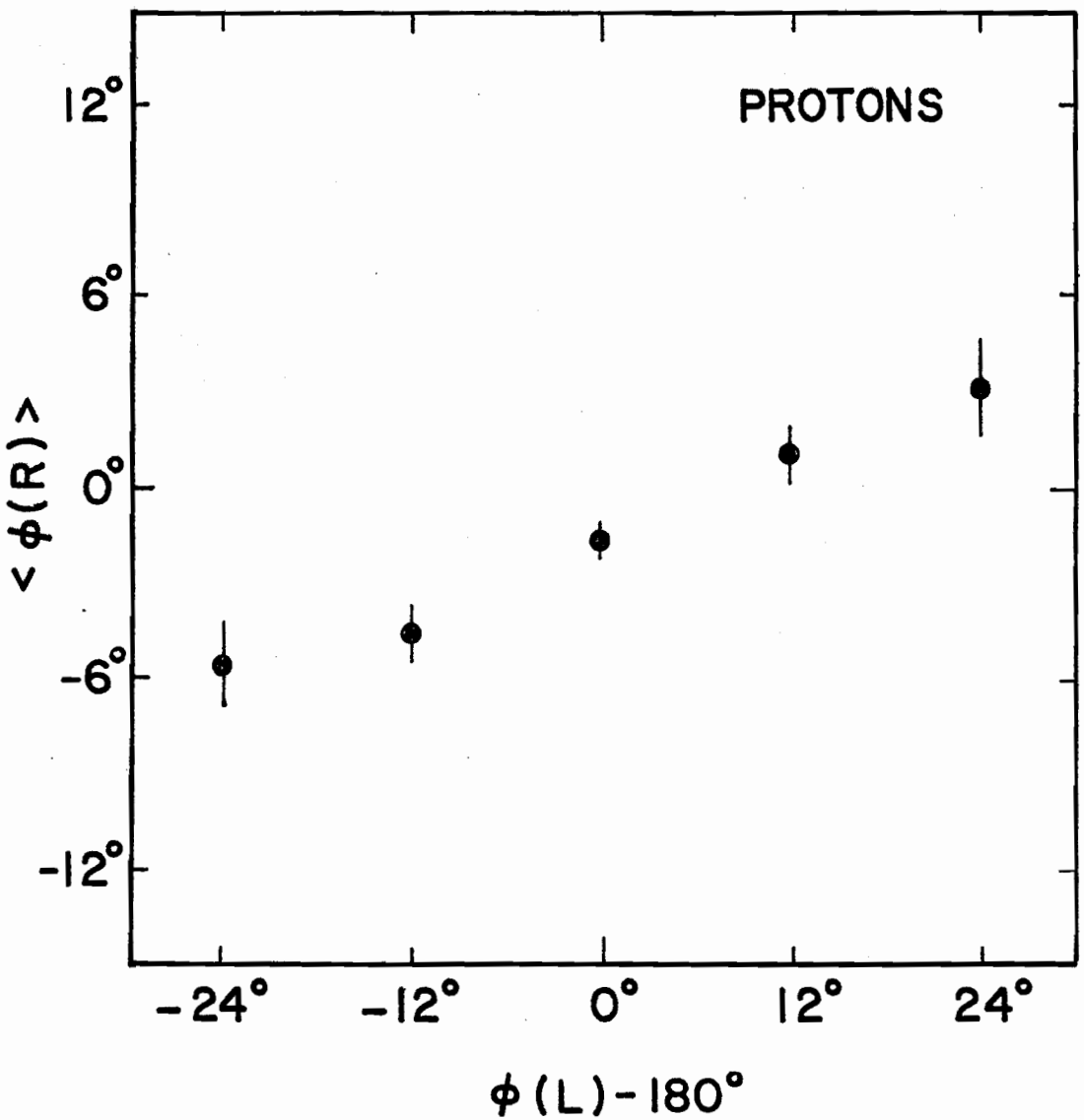

FIGURE 3a

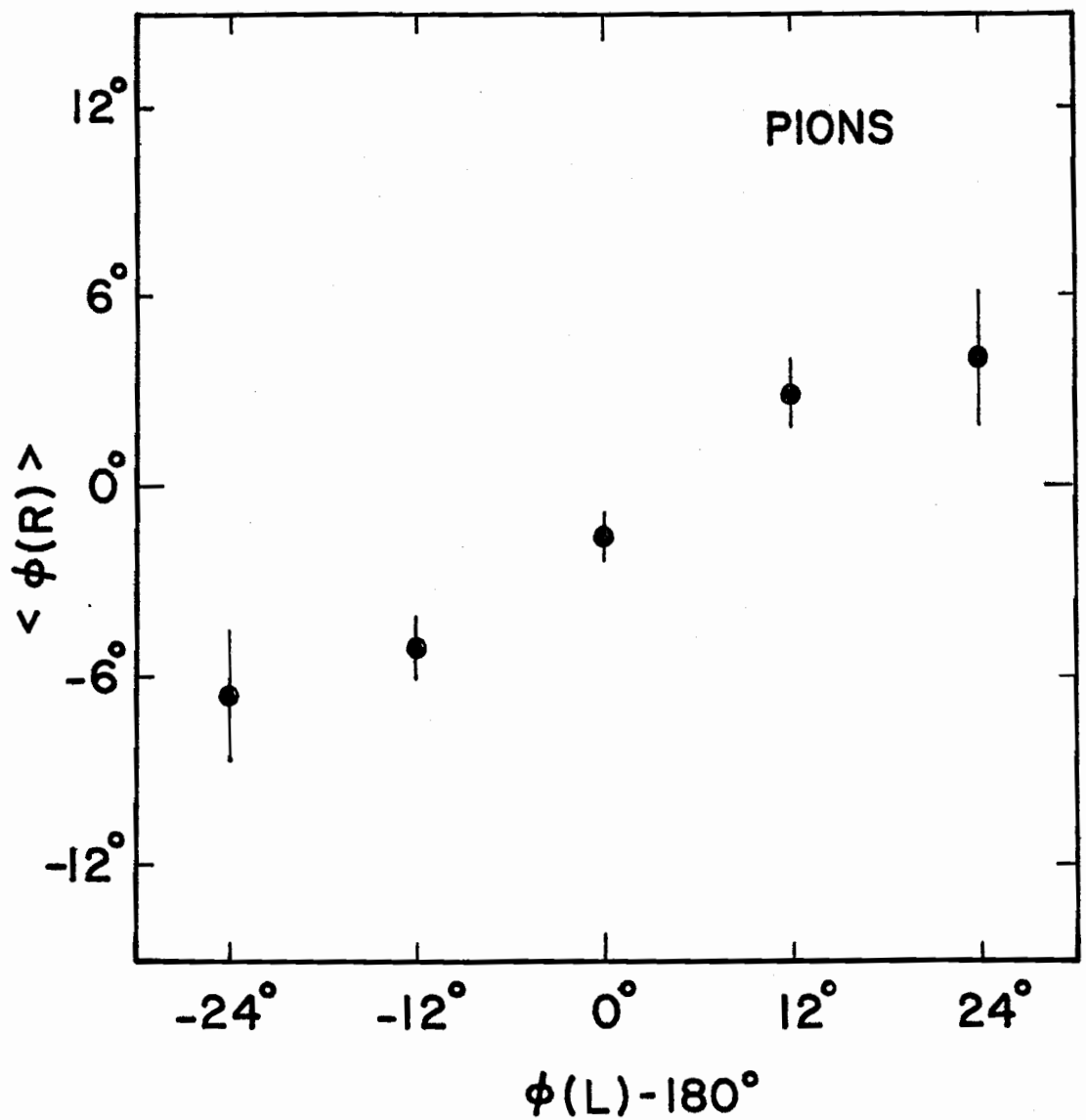

FIGURE 3b

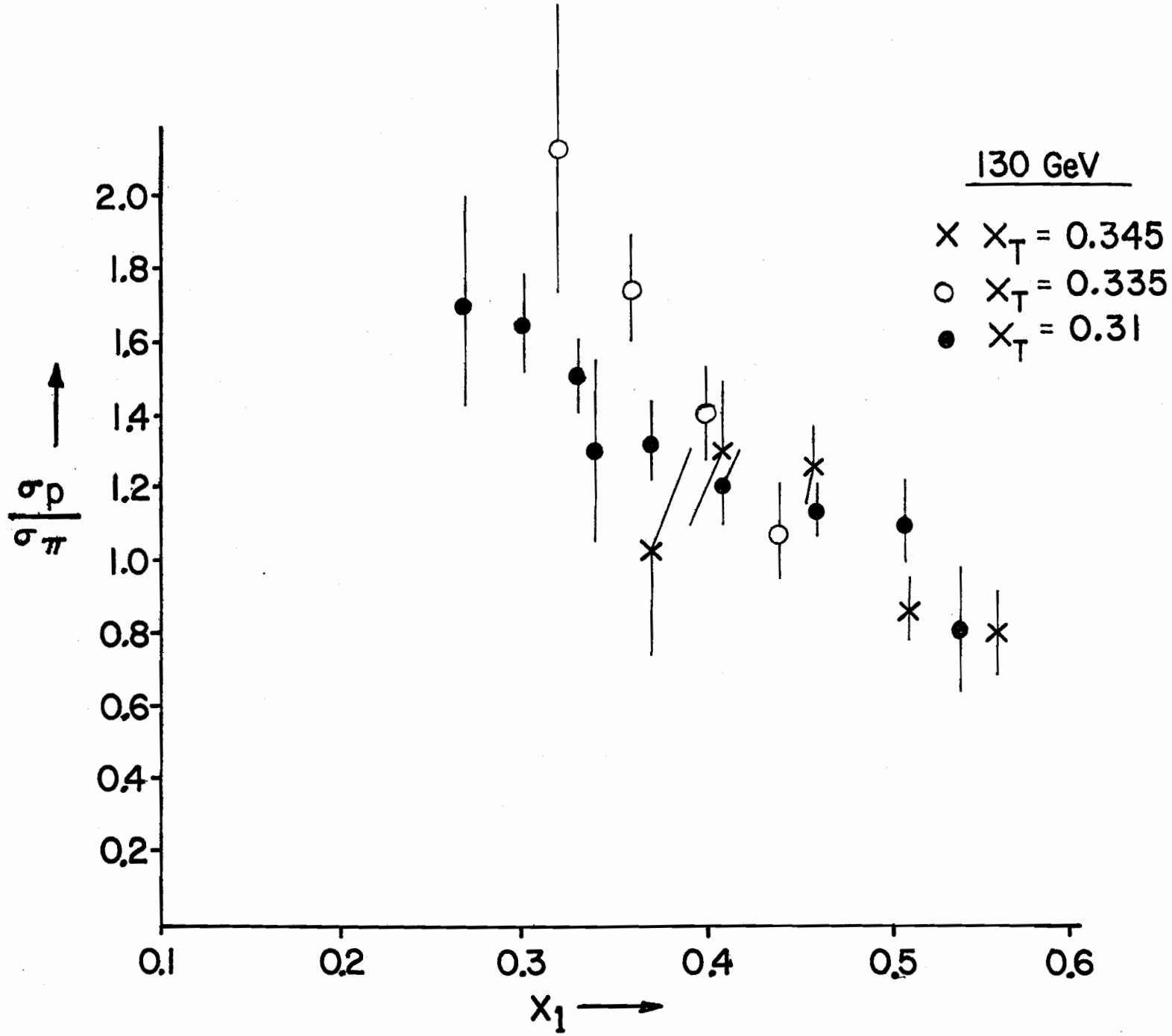
130 GeV
× X_T = 0.345
○ X_T = 0.335
● X_T = 0.31
$\frac{\sigma_p}{\sigma_\pi}$
2.0
1.8
1.6
1.4
1.2
1.0
0.8
0.6
0.4
0.2
0.1
0.2
0.3
0.4
0.5
0.6
X_1

FIGURE 4

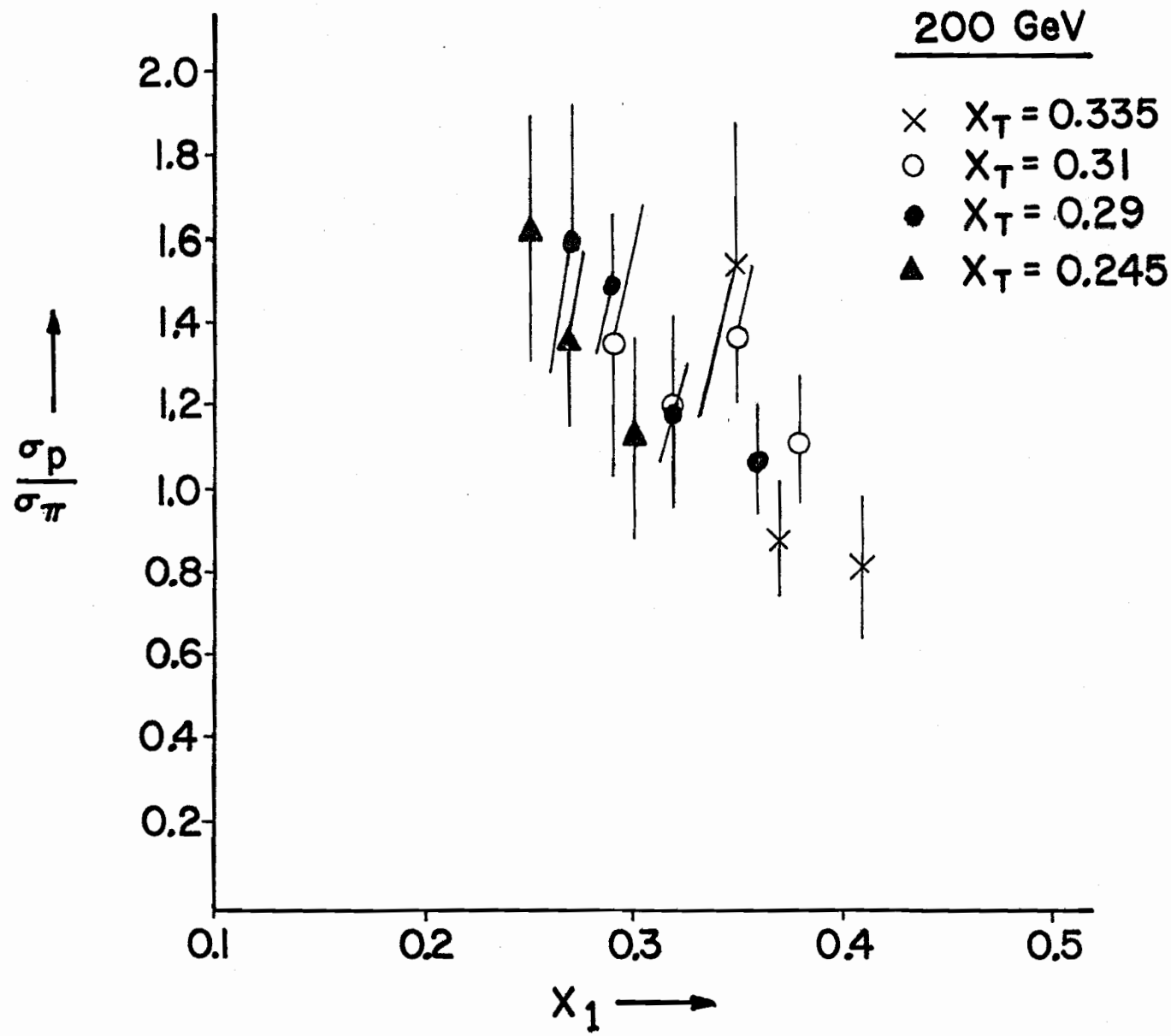
200 GeV
× X_T = 0.335
○ X_T = 0.31
● X_T = 0.29
▲ X_T = 0.245
2.0
1.8
1.6
1.4
1.2
1.0
0.8
0.6
0.4
0.2
$\frac{\sigma_p}{\sigma_\pi}$
0.1
0.2
0.3
0.4
0.5
X_1

FIGURE 5

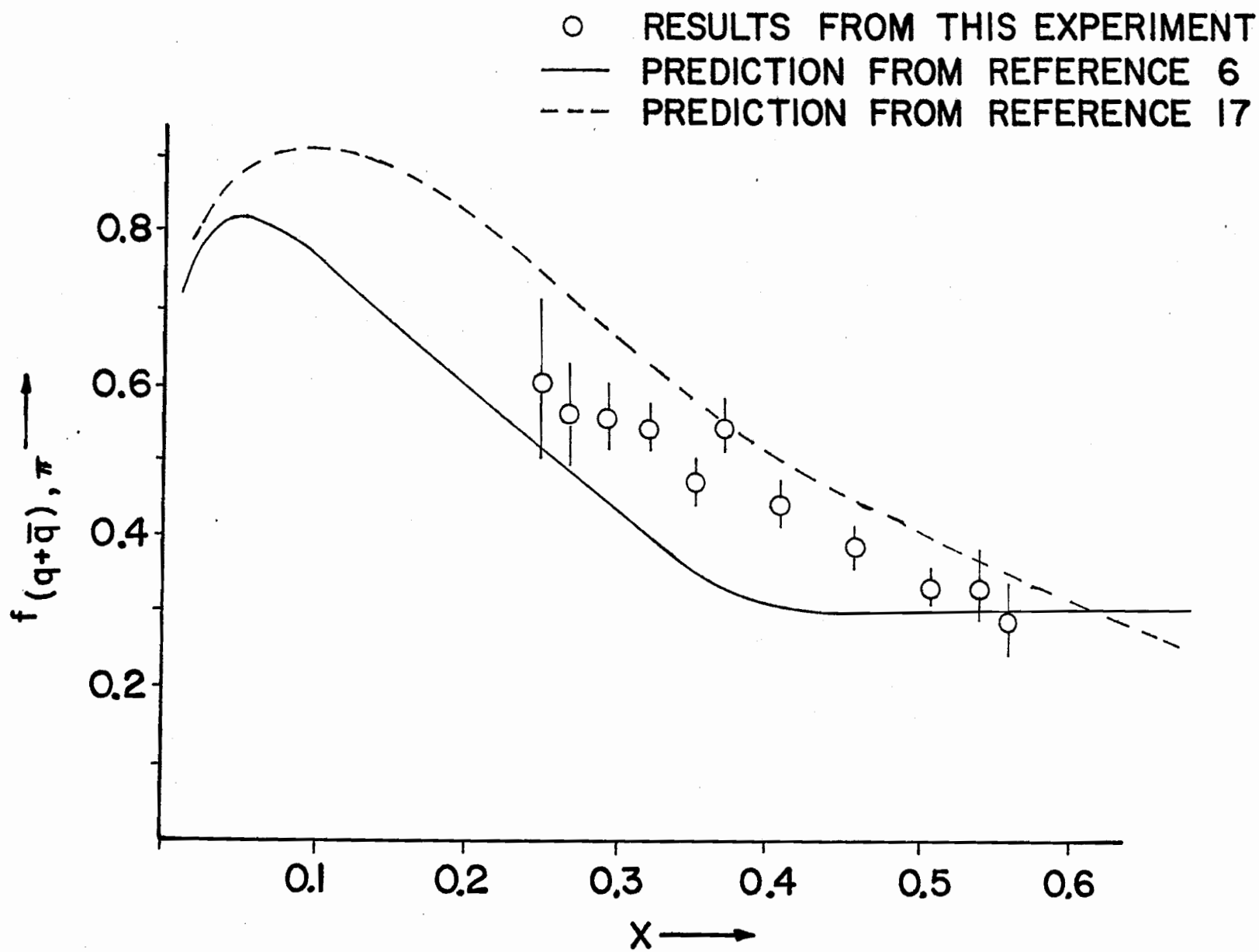
RESULTS FROM THIS EXPERIMENT
PREDICTION FROM REFERENCE 6
PREDICTION FROM REFERENCE 17
0.8
0.6
0.4
0.2
f (q+q̄), π
0.1
0.2
0.3
0.4
0.5
0.6
X

FIGURE 6

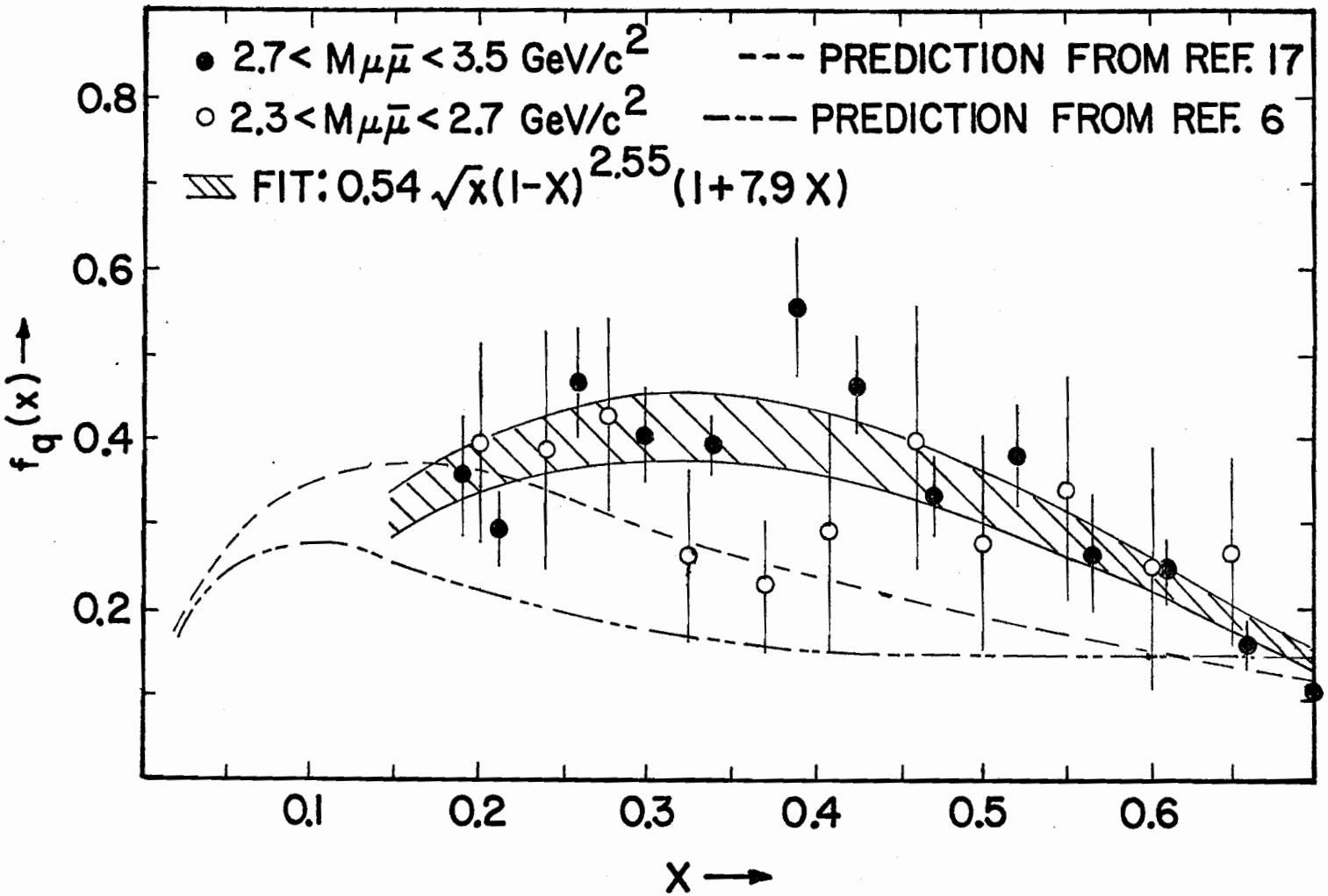
● 2.7< Mμμ̄ < 3.5 GeV/c²
○ 2.3 < Mμμ̄ < 2.7 GeV/c²
FIT: 0.54 √x (1-X)^2.55 (1+7.9 X)
--- PREDICTION FROM REF. 17
---- PREDICTION FROM REF. 6
0.8
0.6
0.4
0.2
f_q(x) →
0.1
0.2
0.3
0.4
0.5
0.6
X →

FIGURE 7